Automated Segmentation of Bioresorbable Vascular Scaffold Struts in Intracoronary Optical Coherence Tomography Images

HHS Public Access

Author manuscript

Int Conf Bioinform Biomed Eng. Author manuscript; available in PMC 2018 August 22.

Published in final edited form as:

Int Conf Bioinform Biomed Eng. 2017 October ; 2017: 297–302. doi:10.1109/BIBE.2017.00-38.

Automated Segmentation of Bioresorbable Vascular Scaffold Struts in Intracoronary Optical Coherence Tomography Images

Junedh M. Amrute

Division of Biology and Biological Engineering California Institute of Technology Pasadena, CA, USA

Lambros Athanasiou, **Farhad Rikhtegar**, and **José M. de la Torre Hernández**

Institute for Medical Engineering and Science Massachusetts Institute of Technology Cambridge, MA, USA

Tamara García Camarero

H.U.M. de Valdecilla, Santander, Spain

Elazer R. Edelman

Institute for Medical Engineering and Science Massachusetts Institute of Technology Cambridge, MA, USA

Abstract

Bioresorbable vascular scaffolds (BVS), the next step in the continuum of minimally invasive vascular interventions present new opportunities for patients and clinicians but challenges as well. As they are comprised of polymeric materials standard imaging is challenging. This is especially problematic as modalities like optical coherence tomography (OCT) become more prevalent in cardiology.

OCT, a light-based intracoronary imaging technique, provides cross-sectional images of plaque and luminal morphology. Until recently segmentation of OCT images for BVS struts was performed manually by experts. However, this process is time consuming and not tractable for large amounts of patient data. Several automated methods exist to segment metallic stents, which do not apply to the newer BVS. Given this current limitation coupled with the emerging popularity of the BVS technology, it is crucial to develop an automated methodology to segment BVS struts in OCT images.

The objective of this paper is to develop a novel BVS strut detection method in intracoronary OCT images. First, we preprocess the image to remove imaging artifacts. Then, we use a K-means clustering algorithm to automatically segment the image. Finally, we isolate the stent struts from the rest of the image. The accuracy of the proposed method was evaluated using expert estimations on 658 annotated images acquired from 7 patients at the time of coronary arterial interventions. Our proposed methodology has a positive predictive value of 0.93, a Pearson Correlation coefficient of 0.94, and a F1 score of 0.92. The proposed methodology allows for rapid, accurate, and fully automated segmentation of BVS struts in OCT images.

Keywords

Optical Coherence Tomography (OCT); Bioresorbable Vascular Scaffold (BVS); K-means clustering

I. Introduction

The profound world-wide impact of coronary artery disease is driven by occlusive plaque burden within the coronary arterial wall [1]. The primary means of addressing these arterial stenoses involves insertion of a metallic stent or bioresorbable vascular scaffold (BVS) [2], [3]. These devices expand and hold open the constricted region enabling once obstructed blood to pass freely [4]. The transition from a focus on invasive bypass-surgery to minimally invasive interventions [3] requires holistic understanding of the effect of different device types on patient cardiovascular function. Metallic stents are accompanied by long-term issues: the relatively inflexible nature of the stent obstructs natural remodeling of the artery and the vasomotion of the artery is not normal [2], [4], [5]. In contrast, BVS hold the promise of enabling early restoration of endothelial functioning, normal vasomotion, and natural remodeling of the coronary artery [6]. In spite of these benefits, concern has been raised for the excess thrombosis and myocardial infarction induced by BVS [7]. Since the BVS technology is recent to the medical community, there is a scarcity of computational methodologies to analyze the quantitative effects of BVS. To achieve this, accurate image representation of the BVS struts and robust stent detection methods are needed.

Optical coherence tomography is an intracoronary imaging technique used to obtain high-resolution images from coronary arteries [8]. OCT is increasingly replacing intravascular ultrasound for coronary imaging, because unlike ultrasound which uses acoustic waves, OCT uses reflected light whose shorter wavelength enables finer resolution [9]. OCT allows detailed morphological assessment of the vessel wall, luminal border, and features associated with increased vulnerability. In light of these benefits, OCT imaging is the primary tool used by clinicians to detect the lumen, characterize plaque and detect devices in coronary arteries *in vivo* [10], [11]. OCT imaging provides high resolution images, which makes it possible to see BVS struts and metallic stents. BVS struts in OCT images appear as well defined rectangular structures having sharp edges while the metallic stents appear as bright fringes with a dark shadow behind.

Although there are several reported methods to detect metallic stent struts [12], [13], to our knowledge, there is only one for detecting BVS struts [14] using OCT images. This approach requires a different methodology to segment malapposed struts and those embedded inside the arterial wall, uses a different percentile based threshold for each patient, and is sensitive to artifacts like blood in the lumen. These drawbacks limit the effectiveness of such a method as many patients have a combination of malapposed and embedded stents and blood artifacts in the lumen [15]. Furthermore, a manual percentile based thresholding procedure is not robust as it assumes similar stent profiles within an OCT pullback and cannot be used across all patients.

To address these shortcomings, we propose a new method based on K-means clustering. The method works for malapposed devices and those embedded inside the arterial wall, automatically detects them, and removes artifacts from the lumen area. In summary, our method involves (Figure 1):

1. sequential raw OCT images acquisition from an OCT pullback,
2. pre-processing of the image to remove the imaging catheter, protective sheath, and guide wire,
3. application of a K-means clustering algorithm, and
4. detection of BVS strut boundaries.

The innovation aspects of the methodology provide

- fully automated methods with no user interaction needed,
- accurate detection of BVS strut borders in the presence of blood artifacts, and
- detection of malapposed and embedded BVS struts.

II. MATERIALS AND METHODS

A. Image Acquisition

The raw OCT image consists of a series of A-lines stored in a matrix, which is in polar coordinates $I(r, \theta)$, where r is the range and θ is the acquisition angle. In order to understand the true form of the image, we convert the image into Cartesian coordinates using the following transformation $I(r,\theta) \rightarrow I(x, y)$ where $x = r\cos(\theta)$ and $y = r\sin(\theta)$.

B. Pre-processing

In the preprocessing stage, a bilateral filter is applied to the image to remove the artifacts.

B.1 Bilateral Filtering—A bilateral filter is a smoothing filter, which preserves edges while reducing overall image noise [16]. The intensity value of each pixel is replaced by a weighted average of pixels in a defined neighborhood, N. The weights in a Gaussian filter depend only on Euclidean distances between neighboring pixels, whereas the bilateral filter also takes into account differences in intensity between neighboring pixels. Incorporating both distance and intensity gradients in the smoothing function ensures that the overall noise is reduced while edge detection is enhanced.

The bilateral filter is defined as:

$$I^f(\hat{x}) = \frac{1}{W_P} \sum_{\hat{x}_i \in N} I(\hat{x}_i) f_r\left(\left\|I(\hat{x}_i) - I(\hat{x})\right\|\right) g_s\left(\left\|\hat{x}_i - \hat{x}\right\|\right) \quad (1)$$

where I^f is the filtered image, I is the raw input image, $\hat{x}$ is the position of the central pixel, $\hat{x}$ each pixel in the defined neighborhood N, f_r is a Gaussian range filter (based on

differences in intensity), g_s is a Gaussian spatial filter (based on Euclidean distances between pixels), and the normalization term W_P is defined as:

$$W_P = \sum_{\hat{x}_i \in N} f_r\left(\left\|I(\hat{x}_i) - I(\hat{x})\right\|\right) g_s\left(\left\|\hat{x}_i - \hat{x}\right\|\right) \quad (2)$$

to ensure the total image energy is preserved [16]. In this methodology, we used a 3×3 kernel window with a σ =1.0 in both Gaussian kernel functions. Several other kernel sizes and smoothing parameters were used, but these gave the best results.

B.2 Artifact removal—Before we start searching for the BVS struts we remove the imaging catheter, protective sheath, and guide wire. To find the start of the catheter in the OCT image (Figure 1, b) we find the first pixel in the first and last column which is above 0.8 intensity units. The lower border of the protective sheath is 0.9 mm (catheter length) below this point, which is ~ 40 pixels. To find the start and end point of the lower sheath border, we use the 40 pixels below the start of the catheter. To detect the outer boundary of the protective sheath we propose an edge detection method, which involves walking along the gradient of the sheath boundary [14]. We construct a weighted, undirected graph from the image matrix and use Djikstra's algorithm [17] to find the minimum cost path.

Each pixel in the image represents a node in the graph and the connectivity between neighboring pixels represents edges in the graph. We use a four-connectivity model [14] such that each pixel is connected to at most four other pixels (top, down, left, and right). Thus, for an $n \times n$ image matrix, there are a total of n^2 nodes and 4(n - 2)2 + 12(n - 2) + 8 edges. We use this expression to pre-allocate memory when constructing the graph in Matlab as it exponentially speeds up the computational run time. To calculate the weights between connected pixels, we use the inverse of the directional gradient:

$$W_x = \frac{1}{G_x} \text{and } W_y = \frac{1}{G_y}, \quad (3)$$

where W_x and W_y are the weights in the horizontal and vertical directions, respectively and G_x and G_y are the intensity gradients in the x and y directions, respectively. As inverse gradient weighting ensures that the strongest edges in the image have the smallest weights we can walk along the gradient by minimizing the cost of weights. To assign weights to edges starting at pixel (i, j) we assign a weight of W^{ij} for all adjacent nodes in the horizontal direction and of W_y^{iJ} for all adjacent nodes in the vertical direction. Using the above formulation, we construct the graph where each structure in the graph is defined by a start node, end node, and node transition cost as defined above. Using the start and end nodes and this graph, we use Djikstra's algorithm to find the minimum cost path.

The region below the guide wire always presents as a black shadow (Figure 1, b). To remove the guide wire, we find the first and last column of the shadow and delete that entire region by:

1. scanning each column and calculating the total intensity of all pixels in a column,
2. marking the first column whose sum falls below 25% of the maximum sum intensity as the start of the guide wire,
3. scanning from the detected guide wire column onwards and marking the first column whose sum intensity rises above that threshold the end of the guide wire, and
4. deleting the entire region between first and last column of the guide wire.

C. Automated Segmentation

To automatically segment the image, we use a K-means [18] algorithm (k = 3 clusters). K-means is an unsupervised machine-learning algorithm used to solve a clustering problem. Given a set of N observations $\{x_1, x_2, \ldots, x_N\}$, the clustering algorithm arranges them into k clusters $S = \{S_1, S_2, \ldots, S_k\}$ to minimize the within-cluster sum of squares.

Formally, we define the optimization problem as a minimization problem [18]:

$$\arg\min_{s} \sum_{i=1}^{k} \sum_{x \in s_i} \|x - \mu_i\|^2, \quad (4)$$

where μ_i is the mean intensity of all the points in cluster S_i. We apply this algorithm to each OCT frame with $k = 3$ clusters and then classify the points into noise (which consists of 2 clusters) and the black background (1 cluster) (Figure 1, d). We tried other cluster values (k = 2, 3, and 4), however, k = 3 gave the highest positive predictive value. To convert this clustered image into a binary image, we find the cluster with the minimum intensity and set this cluster to 0 and all other clusters to 1 (Figure 1, e).

D. BVS Strut Detection

Using the thresholded image (Figure 1, e) we scan down zeach A-line and use the following criteria to classify two points as the start and end points of a BVS strut core:

1. We define the start point as a drop-in gradient from 1 to 0 and end point as a jump in gradient from 0 to 1.
2. We ensure that the pixel distance between the start and end point is within a certain range (based on typical BVS physical specifications).
3. And that the start point of the BVS strut is within a certain range from the lumen border.

Once we find the start and end point of the strut core along each A-line, we mark that region as 1 and all other pixels in that column as 0. This produces a binary image with candidate BVS strut core segments. To eliminate false positives, we remove identified features whose aspect ratio cannot represent a strut and where the object falls below a certain area threshold (noisy pixels). To find the strut outlines, we use a function to outline the perimeter of the candidate segments producing closed polygons in polar coordinates. Finally, we convert

these closed polygons from polar back to Cartesian coordinates to obtain the result (Figure 1, g).

III. DATASET

For the validation of the proposed plaque characterization method we used anonymized OCT examinations from 7 patients. The data were provided by the Hospital Universitario Marqués de Valdecilla, Santander, Spain. The images were acquired using a Frequency Domain (FD - OCT) OCT equipment (LightLab Imaging, Inc) with a 6 Fr FD-OCT catheter (C7 Dragonfly). Automated contrast injection was performed to optimize the best image quality in all pullbacks. An expert manually marked the BVS struts on 658 images which were used as the gold standard for the present study. These images were marked to count the number of BVS struts visible. Then, we ran our methodology to identify strut boundaries and counted the number of struts found. Broken struts and low-quality images were removed from the validation study.

IV. RESULTS

To validate the proposed methodology, the following validation metrics were calculated: Pearson Correlation Coefficient, true positive rate (TPR), positive predictive value (PPV), false negative rate (FNR), false discovery rate (FDR), and F1 score. We denote the true positives as the struts detected by both the methodology and expert, false positives as those struts detected by the methodology, but not by the expert, and false negatives as the struts detected by the expert, but missed by our methodology (Table I).

Additionally, we performed a regression analysis (Figure 2) and a Bland-Altman Analysis (Figure 3). The Bland-Altman analysis revealed a mean of −0.32, which shows no significant bias. Figure 4, shows the number of annotated struts and the number of struts identified by segmentation for each image tested. The overlap between the two curves indicates agreement between the strut detection of the proposed methodology and the struts detected from the annotations and the black non-overlapping regions indicate disagreement Finally, Figure 5 shows our methodology applied to images with extreme noise and a combination of embedded and malapposed struts.

V. DISCUSSION

In this project, we present a fully automated method to detect BVS struts in OCT images. The method robustly removes imaging artifacts, applies a K-means algorithm to automatically threshold the image, and outlines the BVS struts using this thresholded image. The method can be applied to a large number of images and can detect the BVS struts with a PPV of 0.93.

Existing methods in the literature use simplified approaches [14] to remove imaging artifacts and to identify the strut outlines, which introduces post-processing errors in the image-processing pipeline. These methods also require a percentile based thresholding method, which is not robust. Furthermore, these methods rely on a different methodology to identify malapposed struts and embedded struts. Here, we present a fully automated methodology,

which does not require user interaction and can be applied to both malapposed and embedded struts. This is essential since many patients have a combination of malapposed and embedded BVS struts [15]. The time complexity for the method scales as less than 3 seconds per frame when performed on an i7 4 GB RAM machine. This rapid processing is essential as the method is able to provide fast analysis of BVS strut locations.

The exact location of the BVS struts is a clinical parameter of interest. Using these strut locations, clinicians can calculate the diameter of the struts from the lumen and use this information to understand how struts move over time [19]. Temporal tracking is of high importance to understand the efficacy of BVS as certain orientations of the strut may lead to thrombosis [20]. Using this tracking method, and combining it with other techniques (plaque detection) [21] we could potentially predict the trajectory of various struts.

The proposed BVS strut detection method also serves as a foundation for researches who study hemodynamics and rheology inside a stented coronary artery which cannot be defined by any current method. To achieve this, the three-dimensional (3D) configuration of BVS and arterial lumen is needed. Using the proposed method, the BVS struts can be detected in OCT frames and then translated in 3D using well-known 3D OCT reconstruction algorithms [21], [22]. Building patient-specific 3D models will provide clinicians with accurate quantitative metrics to assess patient cardiovascular function post BVS implantation.

VI. CONCLUSION

Accurately characterizing the BVS strut outline is crucial for evaluating the efficacy of BVS in patients. Here, we present a fully automated method to detect the BVS struts in OCT images. The methodology can identify BVS struts with a predictive value of 0.93 and is validated using 658 images. Further research will aim to use these segmentation results to build accurate 3D models and perform computational fluid dynamic simulations. This time efficient segmentation saves time for clinicians and provides a foundation for researchers to translate the BVS in 3D to further understand patient hemodynamics in the coronary artery. More precise definition of structure and hemodynamics provides the opportunity for higher fidelity insight into cardiovascular function not available through direct clinical measurements and may well change our practice of medicine and concept of disease and healing.

Acknowledgment

This project was supported in part by funds to JMA from the Caltech Franz and Anne Nierlich Summer Undergraduate Research Fellowship, Vergottis Fellowship at Harvard Medical School awarded to LA, and R01 support from the National Institutes of Health (GM 49039) to FR and ERE.

*Research supported in part by NIH R01 GM 49039 to ERE and FR, Vergottis Foundation Fellowship to LA and the Caltech Franz and Anne Nierlich SURF Fellowship to JMA.

References

[1]. Roth GA, Huffman MD, Moran AE, Feigin V, Mensah GA, Naghavi M, and Murray CJL, “Global and regional patterns in cardiovascular mortality from 1990 to 2013,” Circulation, vol. 132, no. 17, pp. 1667–1678, 2015. [PubMed: 26503749]

[2]. Brugaletta S, Gori T, Low AF, Tousek P, Pinar E, Gomez-Lara J, Scalone G, Schulz E, Chan MY, Kocka V, Hurtado J, Gomez-Hospital JA, Münzel T, Lee C-H, Cequier A, Valdés M, Widimsky P, Serruys PW, et al., "Absorb Bioresorbable Vascular Scaffold Versus Everolimus-Eluting Metallic Stent in ST-Segment Elevation Myocardial Infarction: 1-Year Results ofa Propensity Score Matching Comparison: The BVS-EXAMINATION Study (Bioresorbable Vascular Scaffold-A Clinical," JACC. Cardiovasc. Interv, vol. 8, no. 1 Pt B, pp. 189–97, 2015. [PubMed: 25616924]

[3]. Ahn JM and Park SJ, "No more debate over left main stenting versus bypass surgery," JACC Cardiovasc. Interv, vol. 9, no. 4, pp. 328–330, 2016. [PubMed: 26892081]

[4]. Maisel WH and Laskey WK, "Drug-eluting stents," Circulation, vol. 115, no. 17, pp. 426–428, 2007.

[5]. Wang Y and Zhang X, "Vascular restoration therapy and bioresorbable vascular scaffold.," Regen. Biom ater, vol. 1, no. 1, pp. 49–55, 2014.

[6]. Bontinck J, Goverde P, Schroë H, Hendriks J, Maene L, and Vermassen F, "Treatment of the femoropopliteal artery with the bioresorbable REMEDY stent," J. Vasc. Surg, vol. 64, no. 5, pp. 1311–1319, 2016. [PubMed: 27462002]

[7]. Kang SH, Chae IH, Park JJ, Lee HS, Kang DY, Hwang SS, Youn TJ, and Kim HS, "Stent Thrombosis With Drug-Eluting Stents and Bioresorbable Scaffolds: Evidence From a Network Meta-Analysis of147 Trials," JACC Cardiovasc. Interv, vol. 9, no. 12, pp. 1203–1212, 2016. [PubMed: 27262860]

[8]. Athanasiou LS, Fotiadis DI, Michalis LK, Atherosclerotic Plaque Characterization Methods Based on Coronary Imaging, 2017.

[9]. Athanasiou LS, Bourantas CV, Rigas G, Sakellarios AI, Exarchos TP, Siogkas PK, Ricciardi A, Naka KK, Papafaklis MI, Michalis LK, Prati F, and Fotiadis DI, "Methodology for fully automated segmentation and plaque characterization in intracoronary optical coherence tomography images," J. Biomed. Opt, vol. 19, no. 2, p. 26009, Feb. 2014.

[10]. Olender ML, Athanasiou LS, de la Torre Hernandez JM, Camarero TG, Cascon JD, Consuegra-Sanchez L, and Edelman ER, "Estimating the internal elastic membrane crosssectional area ofcoronary arteries autonomously using optical coherence tomography images," in 2017 IEEE EM BS International Conference on Biomedical & H ealth Informatics (BHI), 2017, pp. 109–112.

[11]. Tearney GJ, Regar E, Akasaka T, Adriaenssens T, Barlis P, Bezerra HG, Bouma B, Bruining N, Cho JM, Chowdhary S, Costa MA, De Silva R, Dijkstra J, Di Mario C, Dudeck D, Falk E, Feldman MD, Fitzgerald P, et al., "Consensus standards for acquisition, measurement, and reporting ofintravascular optical coherence tomography studies: A report from the International Working Group for Intravascular Optical Coherence Tomography Standardization and Validation," J. Am. Coll. Cardiol, vol. 59, no. 12, pp. 1058–1072, 2012. [PubMed: 22421299]

[12]. Lee S-Y and Hong M-K, "Stent Evaluation with Optical Coherence Tomography," Yonsei Med J http Yonsei Med J, vol. 54, no. 545, pp. 1075–1083, 2013.

[13]. Lu H, Gargesha M, Wang Z, Chamie D, Attizani GF, Kanaya T, Ray S, Costa M. a., Rollins AM, Bezerra HG, and Wilson DL, "Automatic stent detection in intravascular OCT images using bagged decision trees," Biomed. Opt. Express, vol. 3, no. 11, p. 2809, 2012. [PubMed: 23162720]

[14]. Wang A, Nakatani S, Eggermont J, Onuma Y, Garcia-Garcia HM, Serruys PW, Reiber JHC, and Dijkstra J, "Automatic detection ofbioresorbable vascular scaffold struts in intravascular optical coherence tomography pullback runs.," Biomed. Opt. Express, vol. 5, no. 10, pp. 3589–602, 2014. [PubMed: 25360375]

[15]. Gomez-Lara J, Radu M, Brugaletta S, Farooq V, Diletti R, Onuma Y, Windecker S, Thuesen L, McClean D, Koolen J, Whitbourn R, Dudek D, Smits PC, Regar E, Veldhof S, Rapoza R, Ormiston JA, Garcia-Garcia HM, et al., "Serial analysis ofthe malapposed and uncovered struts of the new generation ofeverolimus-eluting bioresorbable scaffold with optical coherence tomography," JACC Cardiovasc. Interv, vol. 4, no. 9, pp. 992–1001, 2011. [PubMed: 21939939]

[16]. Chaudhury KN and Dabhade SD, "Fast and provably accurate bilateral filtering," IEEE Trans. Image Process, vol. 25, no. 6, pp. 2519–2528, 2016. [PubMed: 27093722]

[17]. Dijkstra EW, "A note on two problems in connexion with graphs," Numer. Math, vol. 1, no. 1, pp. 269–271, 1959.

[18]. Bishop CM, Pattern Recognition and Machine Learning, vol. 53, no. 9 2013.

[19]. Nakatani S, Onuma Y, Ishibashi Y, Eggermont J, Zhang Y-J, Campos CM, Cho YK, Liu S, Dijkstra J, Reiber JHC, Perkins L, Sheehy A, Veldhof S, Rapoza R, van Es G-A, Garcia-Garcia HM, van Geuns R-J, and Serruys PW, "Temporal Evolution ofStrut Light Intensity After Implantation ofBioresorbable Polymeric Intracoronary Scaffolds in the ABSORB Cohort B Trial," Circ J, vol. 78, no. 8, pp. 1873–1881, 2014. [PubMed: 24942012]

[20]. Karanasos A, Van Mieghem N, Van Ditzhuijzen N, Felix C, Daemen J, Autar A, Onuma Y, Kurata M, Diletti R, Valgimigli M, Kauer F, Van Beusekom H, De Jaegere P, Zijlstra F, Van Geuns RJ, and Regar E, "Angiographic and Optical Coherence Tomography Insights into Bioresorbable Scaffold Thrombosis: Single-Center Experience," Circ. Cardiovasc. Interv, vol. 8, no. 5, 2015.

[21]. Athanasiou LS, Bourantas CV, Siogkas PK, Sakellarios AI, Exarchos TP, Naka KK, Papafaklis MI, Michalis LK, Prati F, and Fotiadis DI, "3D reconstruction ofcoronary arteries using Frequency Domain Optical Coherence Tomography images and biplane angiography," in 2012 Annual International Conference of the IEEE Engineering in M edicine and Biology Society, 2012, pp. 2647–2650.

[22]. O 'Brien CC, Kolandaivelu K, Brown J, Lopes AC, Kunio M, Kolachalama VB, and Edelman ER, "Constraining OCT with Knowledge of Device Design Enables High Accuracy Hemodynamic Assessment ofEndovascular Implants," PLoS One, vol. 11, no. 2, p. e0149178, Feb. 2016. [PubMed: 26906566]

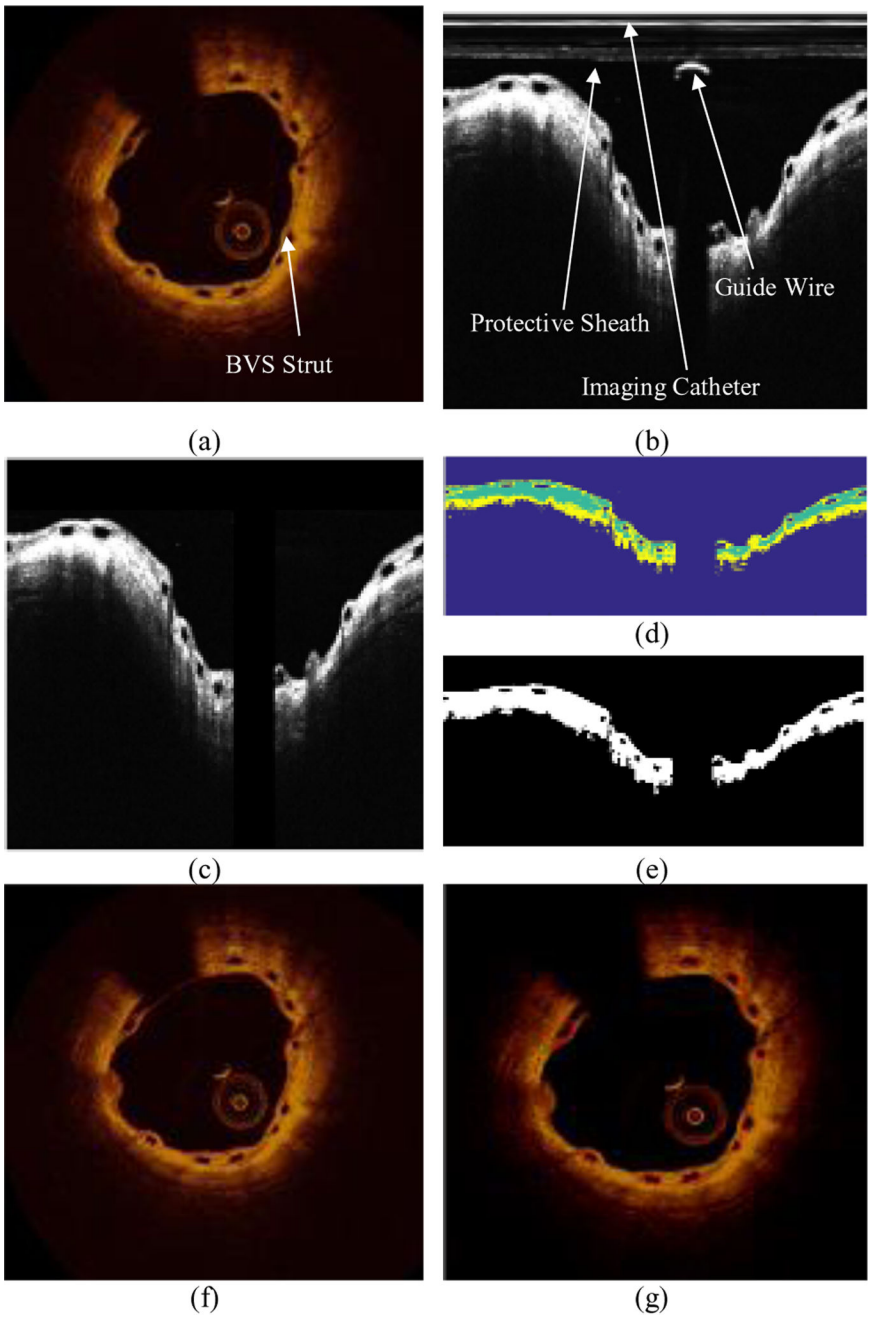

Figure 1.

Overview of proposed BVS strut and lumen detection methodology. (a) Raw OCT image in Cartesian coordinates. (b) Raw OCT image in polar coordinates with true morphology visible. (c) Processed image to remove artifacts. (d) Segmented image using K-means cluster. (e) Thresholded image using K-means result. (f) Segmented lumen border. (g) Segmented BVS strut outline.

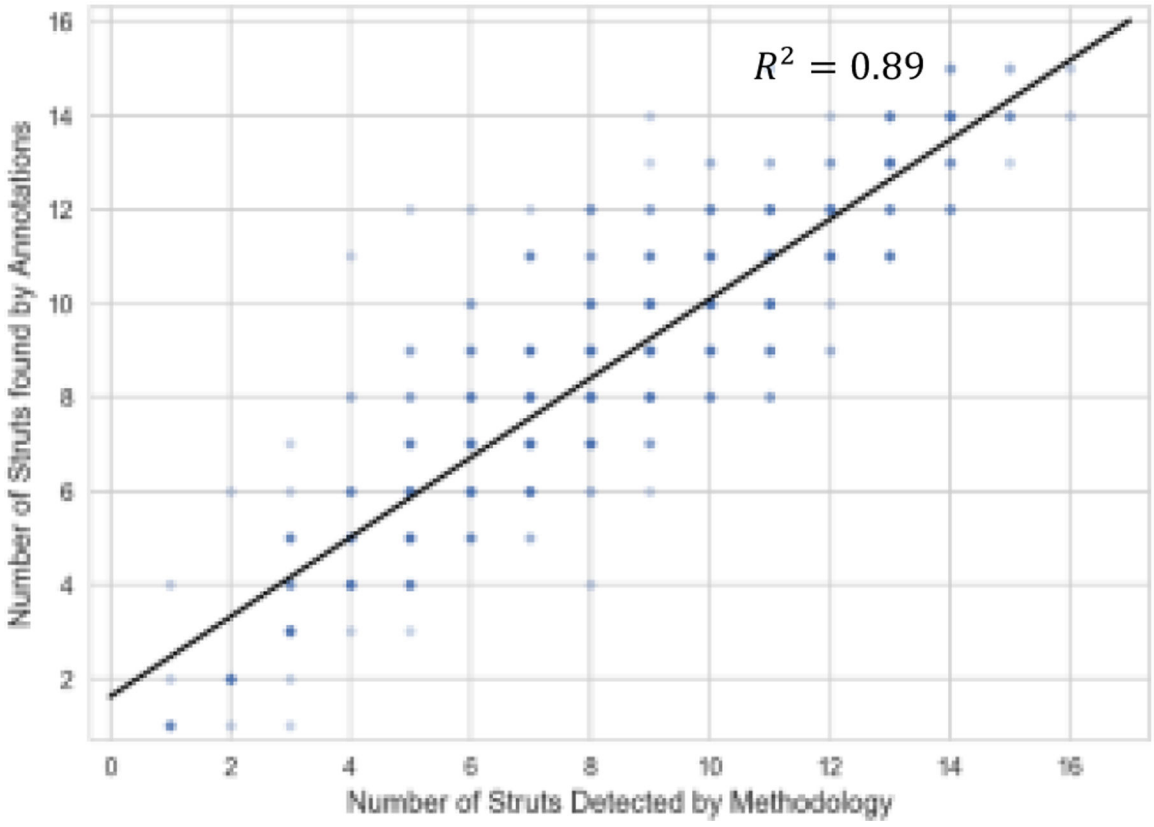

Figure 2.

Correlation graph between the BVS struts annotated by the experts and those detected by the proposed methodology. Using a least squares linear regression an R^2 of 0.89 was obtained with a slope of 0.85 and a y-intercept of 1. In the above regression, we used 658 images and the color density of each point is proportional to the number of data points accumulated at that coordinate.

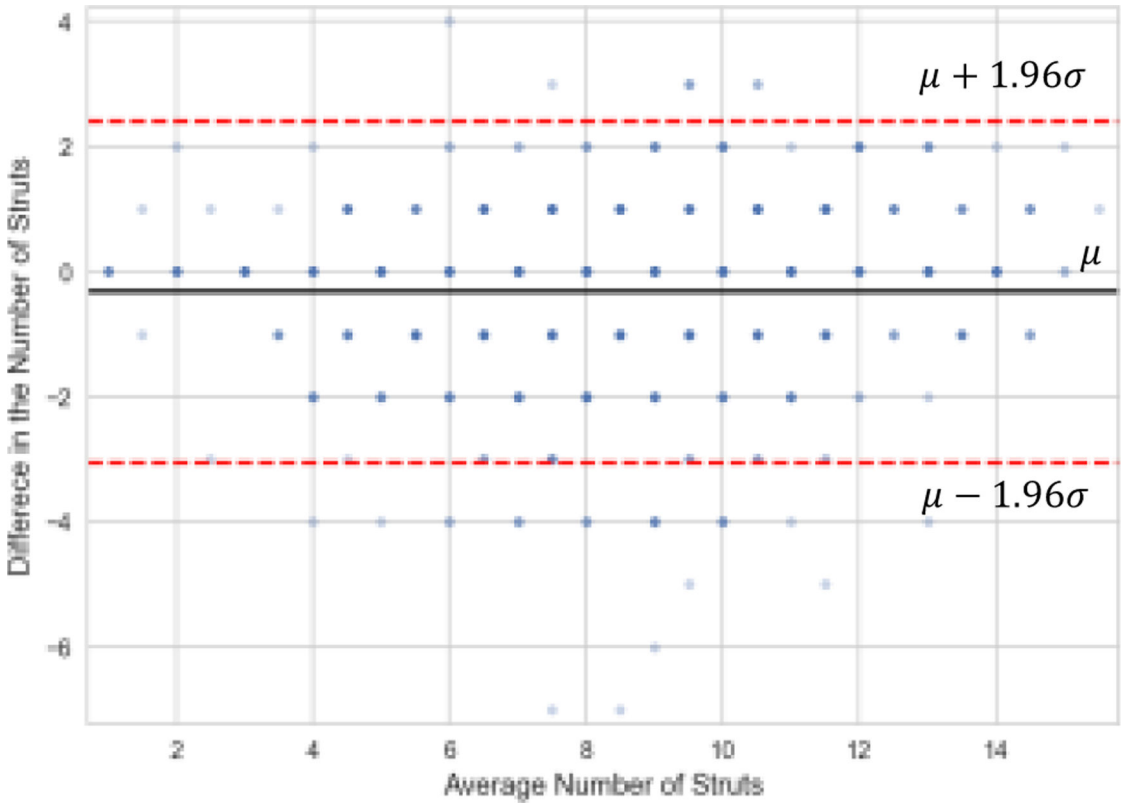

Figure 3.

Bland-Altman analysis plot between the BVS struts annotated by the experts and those detected by the proposed methodology. The average number of struts is defined as the arithmetic mean of the number of struts annotated and the number of struts segmented using the method. The difference is calculated as Number of detected struts using the method − number of annotated struts. The solid black line shows the mean of the difference in the number of struts and was found to be −0.32. The dashed red lines indicate the 95 % confidence interval. In the above analysis, we used 658 images and the color density of each point is proportional to the number of data points accumulated at that coordinate.

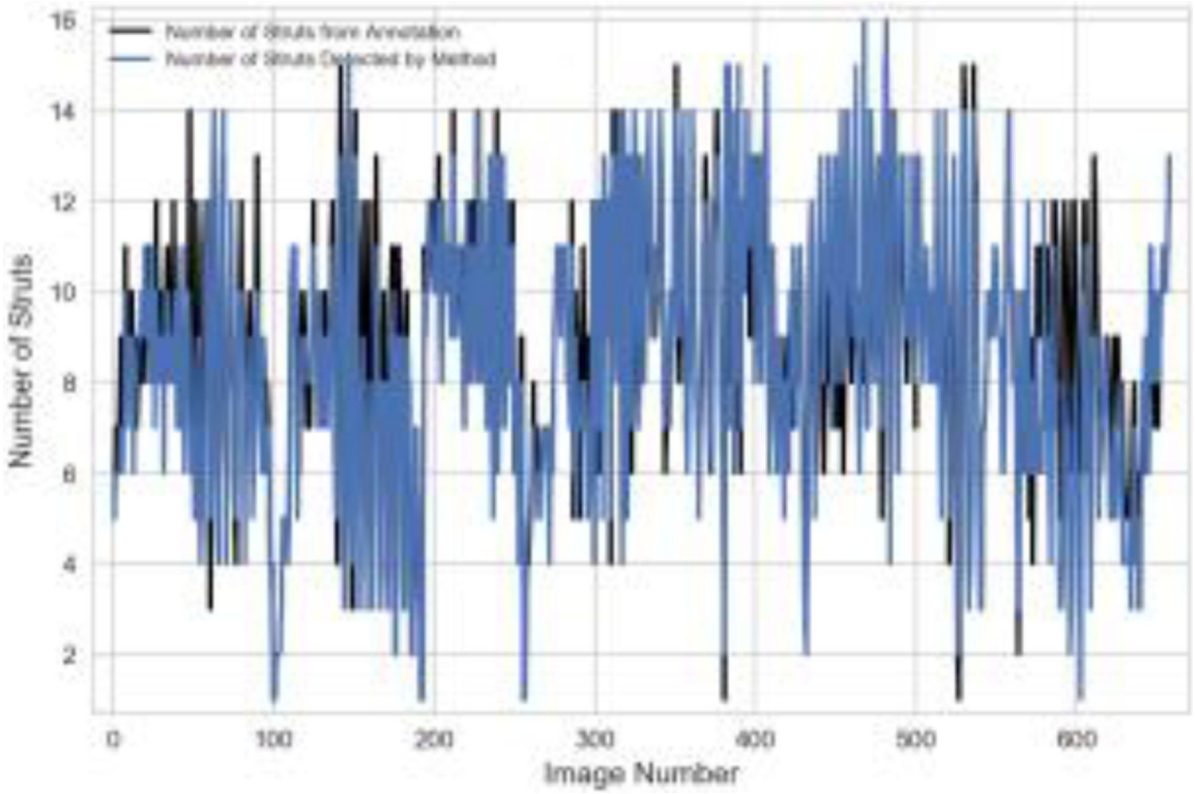

Figure 4.

Plot of the number of annotated struts and number of struts detected by the methodology for each ofthe 658 images used to validate the methodology.

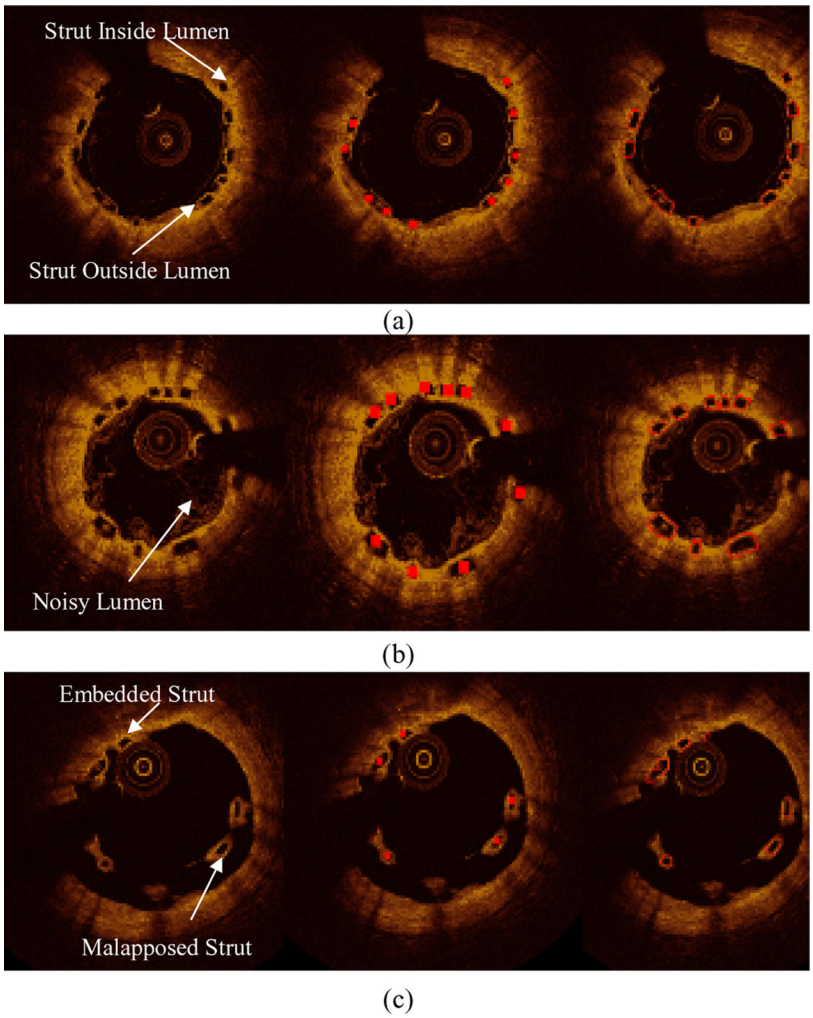

Figure 5.

Examples ofour methodology applied to 3 images from different patients. The first image in each row is the raw OCT image, the second image shows the annotated BVS struts in red, and the third image shows the BVS strut outline detected by our methodology in red. Methodology applied to an OCT image with (a) BVS struts above and below the lumen, (b) a noisy lumen, and (c) embedded and malapposed BVS struts.

TABLE I.

SUMMARY OF VALIDATION METRICS

Validation Metric	Value across 658 images
Pearson Correlation Coefficient	0.94
Positive Predictive Value (PPV)	0.93
True Positive Rate (TPR)	0.92
False Negative Rate (FNR)	0.08
False Discovery Rate (FDR)	0.07
F1 Score	0.92